Ultrafast Electron Transfer in the [Co(Cp)₂|V(CO)₆] Radical Pair

Timothy W. Marin, Bradley J. Homoelle, and Kenneth G. Spears*

Department of Chemistry, Northwestern University, Evanston, Illinois 60208

Received: July 31, 2001; In Final Form: December 18, 2001

We have reexamined our earlier report of electron transfer in the $[Co(Cp)_2|V(CO)_6]$ radical pair using ultrafast infrared transient absorption spectroscopy. The radical pair is created from the $[Co(Cp)_2^+|V(CO)_6^-]$ ion pair by ultrafast visible charge-transfer excitation. Transient absorption experiments with <75 fs resolution reveal two major direct electron-transfer (ET) components with ∼700 fs and ∼5 ps time constants. A small ET component with a ∼75 ps time constant is due to some separation and re-formation of the radical pairs. Transient absorption experiments monitoring the recovery of the ion-pair state show that both fast components are due to ET rather than some other vibrational relaxation (VR) process in the radical state. By modeling the visible charge-transfer band, the two fast ET decay times are assigned to two ion-pair contact geometries with absorption origins different by about 1250 ± 350 cm^{-1}. The ∼700 fs ET lifetime depends on the vibrational quantum state of the nontotally symmetric CO stretch in the $V(CO)_6$ radical, where the lifetime decreases by ∼10% for the first vibrational quantum and ∼45% for the second quantum. There is no quantum effect for the second ion-pair geometry with a 5 ps ET lifetime. Standard ET rate models cannot explain the rate dependence upon vibrational quantum state for a nontotally symmetric vibration, and it may arise from a breakdown of the Condon approximation. We also find that the intramolecular vibrational redistribution (IVR) time to transfer vibrational energy from the totally symmetric CO stretch to the nontotally symmetric stretch is less than 75 fs for a 1-quantum IVR process. This is unusually fast for metal carbonyls and may be assisted by the Jahn−Teller geometry change of the radical. The 2-quantum IVR time is ∼200 fs for 800 and 700 nm charge-transfer excitation wavelengths. At excitation wavelengths of 620 and 555 nm all quantum levels show a 200 fs rise time, which is unexpected for the zero quantum level. We assign this effect to the onset of sufficient internal vibrational energy in low-frequency vibrations to cause geometric interconversion between energetically similar Jahn−Teller geometries in the $V(CO)_6$ radical. The 200 fs rise time is the time for the $V(CO)_6$ radical species to assume a stable geometry, which requires VR of low-frequency vibrations to the solvent. These results demonstrate that earlier measurements from our group on the same molecule had insufficient time resolution to observe the ultrafast ET component and thereby inferred a vibrational quantum effect in a single ET rate of longer duration.

I. Introduction

Electron transfer (ET) is one of the most fundamental physical processes. It is a ubiquitous phenomenon with broad applications in both chemistry and biology. The understanding and control of electron-transfer reactions is one of the most active and extensive research areas of modern day physical chemistry. Many reviews on electron transfer have been published, and we refer the reader to some of those papers for a more comprehensive introduction.[1−7]

Previous measurements made in our laboratory on the ion pair $[Co(Cp)_2^+|V(CO)_6^-]$ (Cp = cyclopentadiene) have shown that ET rates can be dependent on vibrational quantum state.[8] The complex exists in solution at high concentrations in low dielectric constant solvents. It displays a very broad (7040 cm^{-1} fwhm) charge-transfer absorption band centered at 620 nm with a low extinction coefficient of 125 M^{-1} cm^{-1}. Hush analysis[9] of the charge-transfer transition indicates relatively weak electronic coupling of the charge-transfer states, where the coupling value (H_{ab}) of 417 cm^{-1} lies at the upper limit of weak coupling. Optically pumping the charge-transfer band initiates an outer-sphere electron transfer from the $V(CO)_6^-$ anion to the $Co(Cp)_2^+$ cation, forming a radical-pair state. Due to a slight geometry change, the T_{1u} CO stretching modes of the vanadium

hexacarbonyl break down to nearly degenerate E_u and A_{2u} modes and display an energy shift from 1853 cm^{-1} ($\nu = 0$, ion-pair state in CH_2Cl_2) to 1973 cm^{-1} ($\nu' = 0$, radical-pair state). Consequently, the formation of the radical-pair state is observable by growth of the 1973 cm^{-1} band in the infrared absorption spectrum.

Under the Born−Oppenheimer approximation, optical pumping of an electronic absorption is accompanied by vibrational activity in displaced totally symmetric modes. Therefore, growth of the infrared-active CO stretch requires that it must be activated via some other mechanism, which likely involves fast intramolecular vibrational redistribution (IVR) from the higher-frequency totally symmetric A_{1g} mode. From our previous infrared transient absorption measurements[8] and modeling of Raman spectra[10] we have concluded that this IVR process leaves the infrared-active CO stretch with excited vibrational states, and population in quantum levels up to $\nu' = 2$ has been observed experimentally. An estimated anharmonicity of ∼21 cm^{-1} between vibrational quanta in both the ion pair[11] and radical pair allows each level to be monitored individually with some bandwidth overlap from adjacent levels. These excited vibrational states are relatively long-lived, and have IVR and vibrational relaxation (VR) rates that are slower than the back-

Electron Transfer in [Co(Cp)₂|V(CO)₆]

J. Phys. Chem. A, Vol. 106, No. 7, 2002 **1153**

ET rate to the ion-pair state. Thus, back-ET is observable while population still exists in excited vibrational levels.

The $V(CO)_6^-$ anion is a stable 18 electron species and is nearly octahedral in symmetry. The radical species is Jahn–Teller unstable[12] and distorts very easily from an octahedral geometry. We have suggested that after excitation, the unstable radical relaxes to a different symmetry and can distort to many possible geometries, where computations[10] show that the two lowest geometries have D_{3d} and D_{2h} symmetry. Solvent collisions have been proposed to assist conversion between totally symmetric and nontotally symmetric CO stretching modes.

Prior infrared transient absorption experiments measured the back-ET rates for quantum levels $v' = 0$, 1, and 2 in the radical pair with respective decay time constants of 26.4, 11.3, and 5.5 ps, implying a 2-fold increase of the ET rate per vibrational level.[8] Similarly, recovery to the ground state was observable, where the back-ET process leaves the ground state with hot vibrational levels that correlate with the decays of the excited-state population. Levels $v = 1$ and 2 in the ion pair were measured, showing rise times of 18 and 8 ps, respectively. The vibrational quantum dependence of the ET rate in an IR-active mode cannot be explained by standard models,[13,14] which place emphasis only on totally symmetric vibrations. It was concluded that the quantum dependence of the rate may be explainable by a breakdown of the Condon approximation, where the electronic coupling matrix element might increase with vibrational quantum number. Unfortunately, the 2–3 ps time resolution used in these experiments was not fast enough to measure the IVR conversion of the totally symmetric mode to nontotally symmetric modes. Likewise, the time resolution was not fast enough to reveal any ultrafast ET components.

We have conducted new infrared transient absorption measurements with <75 fs time resolution that reveal a new ultrafast (<710 fs) ET component. Measuring the ground-state recovery confirms that the ultrafast component is due to ET and is not an artifact of VR or IVR kinetics in the excited state. The rate has a small quantum dependence, where the rate increases by ~10% for the first vibrational quantum and ~45% for the second quantum. A fast 5 ps ET component has no detectable quantum rate effect. We suggest that the two ET rate components are due to two different ion-pair geometries that have different charge-transfer absorption spectra under a single broad band. The indirect experimental evidence for the two geometries is a relative yield change with excitation wavelength. Models of the charge-transfer band via time-dependent resonance Raman analysis and Franck–Condon calculations support the hypothesis. The quantum effect in the ultrafast ET component could be due to a quantum dependent electronic coupling matrix element arising from breakdown of the Condon approximation. No rise time is apparent for the radical-pair transient absorption when pumping the low-energy side of the absorption origin, thus bounding the IVR time for a 1-quantum conversion of totally symmetric to nontotally symmetric modes to <75 fs. Pumping at energies above the absorption maximum reveals a 200 fs rise time that we assign to Jahn–Teller instability in the $V(CO)_6$ radical. This instability causes lack of a well-defined infrared absorption band until the radical relaxes via solvent collisions to remove the excess vibrational energy in low-frequency modes.

The remaining topics are Experimental, Results, Discussion, and Conclusions. For the reader most interested in electron transfer the main conclusions on electron transfer are in Discussion sections B1 and C. Discussion section B2 contains many technical details of the spectral modeling in multiple subsections, which provide secondary support to the ET conclusions.

II. Experimental Section

The transient absorption apparatus is based on a mode-locked femtosecond Ti:sapphire oscillator and a pulse stretcher/regenerative amplifier/pulse compressor for producing high-power ultrafast laser pulses. Its components are described in prior publications.[15] After compression, pulse widths on the order of 50 fs (fwhm) at 800 nm were observed with a hyperbolic secant squared temporal pulse profile and spectral bandwidth of 27 nm (fwhm). The direct output of a pulse compressor was used for an 800 nm pump beam. Pump beams at 700, 620, and 555 nm were generated from the frequency-doubled output of a laboratory built near-IR optical parametric amplifier (OPA). Pump beam energies were 4.50 μJ/pulse and had a bandwidth of ~15 nm. Autocorrelation of the OPA output shows pulse widths as short as 70 fs. Probe pulses were generated by difference mixing the outputs of two separate near-IR OPA's in a silver thiogallate crystal to produce mid-IR pulses centered at ~5.5 μm (1810 cm⁻¹) with a bandwidth of ~0.65 μm (250 cm⁻¹). Pulses <100 fs are achievable in the mid-IR, as indicated by the rise time of pump/probe electron scattering signals obtained for Ge and InP. Probe beam energies for these experiments were ~10 nJ/pulse. The pump and probe beams were focused at a slight crossing angle of 2° into the sample to give diameters (fwhm) of 600 and 300 μm, respectively. After the sample, the probe beam was re-collimated and focused into a single-grating imaging spectrometer (Spex 270 M, 4 μm blaze grating and modified for thermal stability by removing all electronics from the interior of the spectrometer). A 5 cm⁻¹ band-pass was selected by the spectrometer and imaged onto the photodetector. An indium antimonide photodiode (EG&G Judson J10D) was used for excited-state measurements and a mercury cadmium telluride photoconductive detector (EG&G Judson J15D) was used for ground-state measurements. The photodetector output was sent to a low-noise preamplifier (EG&G-Ortec 142A preamplifier for InSb detector and EG&G Judson PA-100 preamplifier for HgCdTe detector) and the preamplifier output was processed with a boxcar integrator (Stanford Research Systems SR250) and lock-in amplifier (Stanford Research Systems SR850) to provide a voltage suitable for A/D conversion. Every data point was sampled for 100 seconds and averaged over 50 000 laser shots to give baseline noise levels of ~10⁻⁴ absorbance units. Time delays for pump–probe measurements were changed from 34 to 170 fs/pt at about 1–1.5 ps delay and then changed again to 1.7 ps at about 10 ps delay.

Samples of [Co(Cp)₂⁺|V(CO)₆⁻] were prepared via literature methods[16] and were dissolved in dry, filtered dichloromethane (Fisher, distilled over CaH₂). Since the $V(CO)_6^-$ ion is very air and light sensitive, all samples were kept away from room light and under either nitrogen or argon gas during synthesis, preparation, and experiments. Concentrations were 0.03 M for excited-state measurements on the radical pair and 0.006 M for ground-state measurements on the ion pair, where a lower concentration was necessary for the ground-state measurements to allow transmission of the probe beam. Solutions were injected through a syringe filter (Aldrich Teflon syringe filter, 0.22 μm pore size) into a laboratory-built, airtight sample cell. The cell has circular CaF₂ windows and is capable of being continuously rotated during an experiment to minimize local heating of the sample. The cell path length can be varied via use of Teflon

spacers between the cell windows. A path length of 3.2 mm was used for these experiments.

The instrument response function for each experiment was obtained via a pump/probe measurement on a polished germanium window. Visible pumping of the germanium instantaneously creates a transient absorption in the infrared from electron scattering, and the finite pulse widths form a convolution of the infrared and pump beams. By fitting the rise time we find the response function for the experimental conditions. We use a time compensating window identical to the sample cell in front of the germanium sample, which also allows matching the germanium front face to the center of the sample cell. Fits to the response function and all kinetic data were performed with a laboratory-written nonlinear least squares routine and a Levenberg−Marquardt fitting algorithm. Convolution of the excitation pulse was incorporated as a sech^2 response function. Every kinetic component was fully convoluted with the excitation pulse. Typically, the instrument response fit to a pulse resolution of 75−100 fs. The pulse width and time zero (time delay giving maximum temporal overlap of the pump and probe pulses) parameters were fixed for all subsequent runs in each data set.

Review of prior literature has shown that the $v' = 0 \rightarrow 1$ transition for the V(CO)$_6$ radical occurs at 1973 cm^{-1} in dichloromethane.[17] An anharmonicity of 21 cm^{-1} between vibrational levels then places the $v' = 1 \rightarrow 2$ and $v' = 2 \rightarrow 3$ transitions at 1952 and 1931 cm^{-1}, respectively. Pump/probe measurements were performed at each of these frequencies using pump wavelengths of 800, 700, 620, and 555 nm. Previous measurements used 1967, 1946, and 1925 cm^{-1} probe energies and a 620 nm pump wavelength.[8] The current probe energies are thought to lie in better accordance with the actual vibrational information available for V(CO)$_6$. The location of the totally symmetric CO stretch vibration is unknown for V(CO)$_6$, but theory would place it about 100 cm^{-1} higher in frequency near 2073 cm^{-1}. Data collected using a 620 nm pump wavelength also incorporated probe frequencies of 1967 and 1946 cm^{-1} for the sake of direct comparison with our prior data. Each pump wavelength represents a different experimental set. At each pump wavelength, all probe frequencies were collected sequentially using the same sample with the exception of the 1931 cm^{-1} probe at 620 nm. During each experimental set, the laser was not changed so that direct comparison could be made between vibrational quanta at each pump wavelength without added variables from differences in laser power and pulse width.

The ground-state IR absorption width is 45 cm^{-1} fwhm,[10] and it is likely to have heterogeneous components from octahedral distortion and from two ion-pair geometries (see later discussion). If the radical pair has a similar bandwidth per vibrational level, the nominal 21 cm^{-1} change in probe wavelength between vibrational levels would give signals with up to 50% contribution from adjacent levels. In this case the observed transient decays would be a mixture of decays for adjacent levels. However, one can observe large changes in the kinetics between most adjacent levels, which suggests that the radical species has a narrower line width, possibly due to weaker interaction in the radical pair (see later discussion).

The $v = 0 \rightarrow 1$ ground-state transition lies at 1853 cm^{-1},[10] placing the $v = 1 \rightarrow 2$ and $v = 2 \rightarrow 3$ transitions respectively at 1832 and 1811 cm^{-1}. Information on the $v = 0 \rightarrow 1$ transition is unobtainable due to very low probe beam transmission at this frequency, thus the ground state was probed only at 1832 and 1811 cm^{-1}. The signals observed for the hot ground-state absorptions (positive ΔA) compete with the ground-state bleach
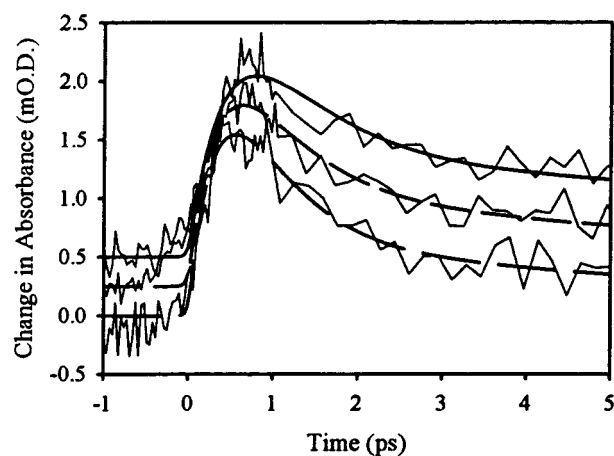

Figure 1. Infrared transient absorptions and data fits for the [Co-(Cp)$_2$|V(CO)$_6$] radical pair after 620 nm excitation. The decays are assigned to back-electron transfer to form the ion pair. Decays from quantum levels $v' = 0$ (1973 cm^{-1}, solid fit), $v' = 1$ (1952 cm^{-1}, short dashed fit), and $v' = 2$ (1931 cm^{-1}, long dashed fit) are shown with normalized amplitudes. The signals are dominated by a <400 fs decay. The time axis has time delay increments of 34 and 170 fs/point, with finer time increments for the early part of the curve.

(negative ΔA) at these probe frequencies, producing very small changes in net absorption. Therefore an 800 nm pump beam with an energy of 80 μJ/pulse and a stretched (by compressor adjustment) pulse width of ~1.7 ps was used to produce signals larger than the nominal baseline noise level of 10^{-4} absorbance units. A stretched pump beam was used in order to prevent nonlinear optical processes in the sample and cell windows. The 1.7 ps convolution of the pump and probe beams was measured via the germanium calibration, where the response function is dominated by the pump beam duration since the probe beam is ~75 fs.

Temperature-dependent electronic absorption spectra for the [Co(Cp)$_2$$^+$|V(CO)$_6$$^-$] ion pair were obtained with a diode-array UV/Vis spectrophotometer (Hewlett-Packard 8452 A) equipped with a liquid nitrogen cryostat and temperature controller (Oxford ITC4). A sample concentration of 0.005 M was used and the cell path length was 1 cm. Spectra were obtained at temperatures from 296 K down to 173 K in ~20 K increments.

III. Results

The normalized radical-pair transient IR absorptions obtained with a 620 nm pump are shown in Figure 1 for probes at $v' = 0$, 1, and 2. In Figure 1 the time delay is stepped from 34 fs/point to 170 fs/point at ~1 ps past the peak, and the plots are offset for clarity. The rising edge shows evidence of free induction decay (see later discussion), which is greater for $v' = 2$, when the probe wavelength is nearer the ground-state frequency at 1853 cm^{-1}. Table 1 summarizes the fits to the transient absorbance data for all pump and probe wavelengths. At all pump wavelengths, three distinct decays are observable for each transient. We find a large amplitude ultrafast component in the <700 fs range (τ_1), a similar amplitude fast component on the 5 ps range (τ_2), and a very small amplitude long time scale component in the range of 75 ps (τ_3). Decay time uncertainties are ±75 fs for τ_1, ±1 ps for τ_2, and ±25 ps for τ_3. Amplitude uncertainties are ±0.05. The data precision was insufficient to independently fit the rise time of τ_2 unless the rise time was greater than ~400 fs. Since no signals required an independent rise time for τ_2, we assumed equal rise times for both components. The kinetic fits are not consistent with the large amplitude ultrafast decay (τ_1) decaying into a rising

Electron Transfer in [Co(Cp)₂|V(CO)₆]

J. Phys. Chem. A, Vol. 106, No. 7, 2002 **1155**

TABLE 1: Parameters from Transient Absorption Fits[a]

	800 nm pump			700 nm pump			620 nm pump					555 nm pump		
	1973 cm⁻¹	1952 cm⁻¹	1931 cm⁻¹	1973 cm⁻¹	1952 cm⁻¹	1931 cm⁻¹	1973 cm⁻¹	1967 cm⁻¹	1952 cm⁻¹	1946 cm⁻¹	1931 cm⁻¹	1973 cm⁻¹	1952 cm⁻¹	1931 cm⁻¹
τ_1	0.69	0.62	0.44	0.71	0.66	0.45	0.41	0.40	0.35	0.28	0.25	0.38	0.27	0.22
rise time	<0.07	<0.07	0.19	<0.07	<0.11	0.23	0.20	0.23	0.21	0.22	0.24	0.24	0.21	0.20
τ_2	6.0	4.8	6.2	4.6	4.5	5.9	3.9	4.0	4.2	4.5	3.6	4.7	4.2	4.5
rise time	<0.07	<0.07	0.19	<0.07	<0.11	0.23	0.20	0.22	0.19	0.21	0.25	0.24	0.20	0.19
τ_3	95	98		91	78	130	64	50	66	62	58	87	49	46
rise time	<0.07	<0.07		<0.07	<0.11	0.23	0.20	0.23	0.20	0.21	0.25	0.24	0.23	0.19
amplitude τ_1	0.53	0.56	0.89	0.50	0.54	0.79	0.64	0.73	0.78	0.83	0.97	0.75	0.87	0.98
amplitude τ_2	0.35	0.34	0.11	0.45	0.34	0.12	0.24	0.18	0.18	0.13	0.02	0.18	0.09	0.01
amplitude τ_3	0.12	0.10		0.05	0.12	0.08	0.12	0.09	0.04	0.04	<0.01	0.07	0.04	0.01

[a] ET times for τ_1, τ_2, and τ_3 are all in ps. Amplitudes are normalized to unity at each probe frequency.
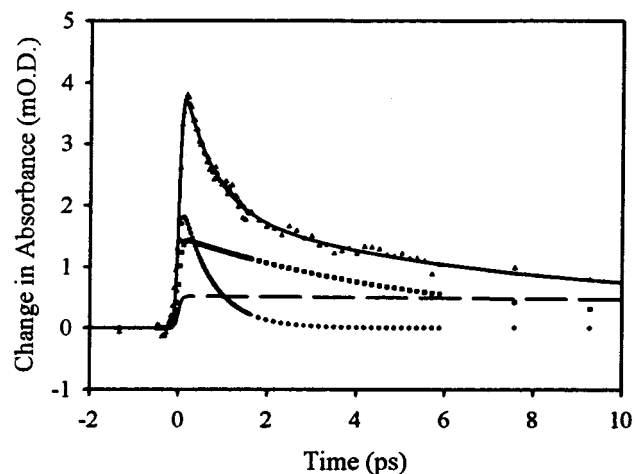
Figure 2. Infrared transient absorption for the [Co(Cp)₂⁺|V(CO)₆⁻] radical pair for a 800 nm pump and probe at $v' = 0$. The three components needed to fit the raw data (triangles) are shown with decay times 690 fs (τ_1, diamonds), 6.0 ps (τ_2, squares), and 95 ps (dashed line). Individual components sum to give the solid line.

TABLE 2: Absorbance Changes for the [Co(Cp)₂|V(CO)₆] Radical Pair Observed at Each Pump/Probe Combination and Their Normalized Relative Values

pump wavelength (nm)	obsd total abs change (mO. D.)			rel abs change		
	$v' = 0$	$v' = 1$	$v' = 2$	$v' = 0$	$v' = 1$	$v' = 2$
800	3.8	3.2	2.6	0.40	0.33	0.27
700	2.9	2.1	1.3	0.46	0.33	0.20
620	1.7	1.7	1.7	0.33	0.33	0.33
555	2.1	2.9	1.5	0.32	0.44	0.23

component with a longer decay (τ_2). As we discuss later, a decay correlating with a rise would be expected for the lowest energy transition originating from $v' = 0$ if the two components were associated with a single species undergoing vibrational relaxation.

Figure 2 displays the contributions of the various fitting components. Table 2 shows the actual and relative absorbance changes observed at each pump wavelength. The relative amplitudes of τ_1, τ_2, and τ_3 are not constant with quantum number and pump wavelength. On average the relative signal amplitudes assigned to τ_1 for $v' = 0$, 1, and 2 scale respectively as ~60%, 70%, and 90%. The amplitude ratio of τ_1 to τ_2 is similar for 800 and 700 nm pump wavelengths with a value of ~1.3:1.0 for $v' = 0$, but it increases to 2.7:1.0 and 4.2:1.0 with 620 and 555 nm pumps.

We measured one infrared spectrum at an excitation wavelength of 620 nm by scanning infrared wavelengths on the monochromator at a fixed delay of 100 fs. We found that the highly overlapped infrared absorption region gave no clear spectral peaks. This is in contrast with kinetic parameters of Table 1, where there are significant changes with probe wavelength. The overlapped infrared features are not unexpected if they have contributions from two geometries (see later discussion).

The data show some unusual rise time trends as a function of quantum number and excitation wavelength that relate to VR and IVR processes. A ~200 fs rise time is observable for all probe frequencies at 620 and 555 nm and for level $v' = 2$ at 800 and 700 nm. No rise time is resolvable (<75 fs) for $v' = 0$ or 1 at 800 and 700 nm, but at $v' = 2$ a 200 fs rise time became apparent. Overlaps of infrared absorption bands could cause an averaging effect for the different quantum levels. However, this effect cannot be too severe since there is a clear demarcation between the $v' = 1$ and $v' = 2$ transients, where a ~200 fs rise time is required for $v' = 2$ and not for $v' = 1$. In the case of $v' = 1$, simulation of the experimental noise suggests that up to 15% of the total signal amplitude could have an unresolved rise time, which defines the possible effects of bandwidth overlap. This change in character is evidence that the overlap of adjacent levels in the V(CO)₆ radical is not as great as suggested by the ground-state bandwidth. Several measurements were taken at polarization angles between the pump and probe different from the normal 54.7°, but all polarizations gave the same transients so motional effects or other polarization effects are not present in the transients.

The data show a vibrational quantum dependence of the ET rate for component τ_1. Averaged over all pump wavelengths, the ET time decreases by ~20% for the first vibrational quantum and ~35% for the second quantum. As we shall show later, the observed times at 800 and 700 nm are likely to have fewer interpretive issues, and the decreases per quantum level are ~10% and 45%. No quantum dependence is discernible for τ_2 where a 20% or more change in the ET time should be observable within our signal-to-noise level.

The assignment of particular transients to either ET or other VR processes requires measuring the recovery of the ground-state ion pair, which must result from back-electron transfer. Figure 3 shows a ground-state transient absorbance measurement for the ion pair where the $v = 2 \rightarrow 3$ transition of the CO stretch is monitored with an 1811 cm⁻¹ probe and 800 nm pump. The positive absorption signal is assigned to the $v = 2$ excited vibrational level that exists in the ground state after ET. This hot ground-state absorbance competes with bleaching of the ground-state absorption band at 1853 cm⁻¹ to give a very small overall signal. Within the high baseline noise for the small signal, the absorption bleach of the ground-state band is not observed prior to the evolution of the transient absorption. This is expected for a 1.7 ps response time if the rise time of the
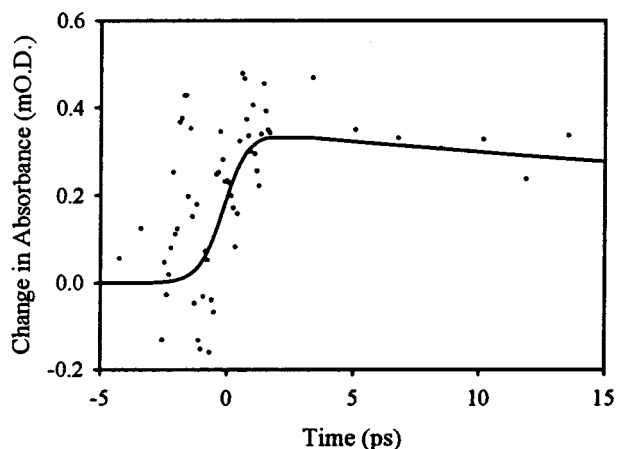
Figure 3. Infrared transient absorption for the $[Co(Cp)_2^+|V(CO)_6^-]$ ion pair after back-electron transfer. The transition for $v = 2$ is shown. The rise time is limited by the 1.7 ps resolution of this particular experiment.

Figure 4. Filling models of the $[Co(Cp)_2^+|V(CO)_6^-]$ ion pair where (a) three oxygen atoms contact the top of the Cp ring and (b) where two oxygen atoms contact the cleft between the two Cp rings.

transient is much less than 1.7 ps. *If the 5 ps ET component provided the only path for returning to the ground state while the ultrafast component was a vibrational relaxation feature, then a clear ∼5 ps rise time would have been visible.* For the case of two components a kinetic model with a 1.7 ps response function shows that the rise time for the longer-lived component should not be obvious in the presence of a larger ultrafast rise time, and would be unobservable with any signal-to-noise ratio less than ∼10. This model uses estimates from Franck−Condon Factors (FCF's) and the observed amplitudes of the two ET components to show that if both components are ET then about 30% of the signal would have a 5 ps rise time. Therefore, this experiment is sufficient to demonstrate that an ultrafast ET path is present with significant amplitude. This identifies τ_1 and τ_2 with ET rather than a mixture of fast vibrational relaxation in τ_1 and ET in τ_2. Probing the ion-pair $v = 1 \rightarrow 2$ transition at 1832 cm^{-1} gives similar results, but the signals are slightly noisier.

The expected coherence artifact[18,19] is observable in many of our experiments and causes an apparent negative shift of time zero and an additional rise time before time zero. Our germanium calibration experiment allows a reliable measure of the rise time resolution and time zero, so that we can identify the minimal delay time for not having coherence effects. The coherence effects are greater when the probe wavelength is closest to the ground-state infrared absorption. Consequently, absorption transients for $v' = 0, 1$ with offsets of 120 and 100 cm^{-1}, have minimal rise time distortion, and accurate rise time fits are possible. When the coherence artifact is present, oscillatory behavior often is present in the rise time.

IV. Discussion

A. Overview. Charge-transfer excitation creates a radical pair that instantaneously retains the ion-pair geometry. Prior resonance Raman and vibrational analysis[10] demonstrated that the excitation is a standard case of FCF activity in totally symmetric vibrations, where we expect totally symmetric CO stretching mode activity in the V(CO)$_6$ radical. The transient processes in the radical pair begin with IVR conversion of the totally symmetric CO stretching vibration to nontotally symmetric IR-active stretching vibrations. The data demonstrate that the IVR conversion one vibrational quantum to the IR-active mode is <75 fs. The ET rates are for a vibration in the IR active mode, and the primary mechanistic problem is explaining two decay
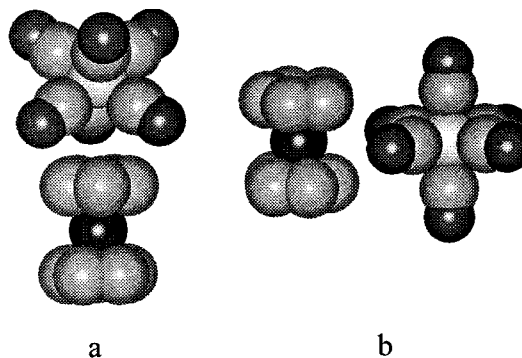
rates with similar amplitudes and times of 700 fs and 5 ps. A third ∼75 ps component was assigned to a small amount of radical separation and re-formation.

As briefly discussed in the results section, the ground-state recovery data is the best evidence that both fast components involve ET. Furthermore, we show that assigning the 700 fs and 5 ps decay to VR and ET, respectively, is inconsistent with the kinetics. Other geometric changes such as relative rotation of the radicals cannot account for rapidly creating the 700 fs (τ_1) and 5 ps (τ_2) decay components in similar amounts. With the experimental time resolution, such motion would have to occur on a <75 fs time scale, which we show is unlikely from the moments of inertia of the vanadium carbonyl radical.

Therefore, we propose that two geometries are present to account for two rates. However, we can only indirectly test this hypothesis by making experimental comparisons with the wavelength dependence of component intensities predicted by absorption spectral models. In our spectral modeling we analyze the electronic absorption spectrum, Raman spectra, ab initio computed models for ion pairs and radical pairs in solvent, FCF computations, FCF's from the observed radical populations, and changes in populations and ET rates with excitation wavelength. We use these data to show that two ion-pair geometries could be in equilibrium, where they each have a unique ET rate and a charge-transfer absorption spectral offset of ∼1200 cm^{-1}. Two candidate geometries are shown in Figure 4, and they are discussed later in more detail.

The data show that at shorter wavelengths there is an onset of a new process identified by a rise time in the transient IR for all quantum levels. We interpret the rise time as a stabilization time for multiple V(CO)$_6$ geometries, where multiple geometries could be interconverting until VR transfers low-frequency vibrational energy to the solvent. The V(CO)$_6$ radical is a Jahn−Teller distorted species created from the nearly octahedral ion geometry in the ion pair, and ab initio computations identify two such structures that lie close in energy, and others may be accessible with similar energy. Spectral modeling shows that the rise time onset correlates with pump wavelengths that leave greater excess energy in the radical pair.

Another outcome of the analysis is that the vibrational quantum dependence of the ET rate is less than inferred from our prior measurements due to the inadequate time resolution of those experiments. The quantum effect for the 700 fs component is a ∼10% increase from $v' = 0$ to $v' = 1$ and a ∼45% increase from $v' = 1$ to $v' = 2$. There is no quantum effect for the 5 ps component.

The following section B1 discusses the experimental evidence for two geometries and the information on IVR and VR present

in our data. Section B2 provides a technical discussion of an absorption model for two components and its predictions for kinetic effects at various wavelengths. This is necessarily complex, and not required for those readers interested in the trends of ET rates. The ET rates are discussed in section C, with emphasis on the vibrational quantum effects being too large for explanation by standard models. This section also makes comparisons with prior experiments.

B1. Origin of Multiple ET Rates. *Two Geometries and Vibrational Relaxation Processes.* The observation of multiple decay rates for ET is not consistent with first-order kinetics from a single species. The two shortest components are of most interest for ET, while the low-amplitude 75 ps component (τ_3) is explainable by radical-pair separation and diffusion to re-form a contact radical pair that then undergoes ET. This component probably originates from the 5 ps component, since greater probability of radical separation becomes more likely on this time scale than for the faster 700 fs component. A more definite example of ion-pair diffusion in a related compound was demonstrated by changing solvent viscosity over a wide range to affect the yield.[20] An alternative possibility is a small probability of spin change in the radical pair that slows the ET, and such processes have been seen for a radical pair with Co-(CO)$_4$.[21] The data for τ_3 show a slow return to a noisy baseline, and the time constants and amplitudes have large error limits. The times are generally less than 100 ± 25 ps and the baseline noise makes it difficult to be very precise on these values.

In Table 1 the two components τ_1 and τ_2 often are of similar amplitude. Our earlier discussion emphasized that ground state recovery kinetics established both decays as ET, but we briefly examine an alternative vibrational relaxation hypothesis to show its inconsistency with the data. In this model the two decays can be assigned to a single species with a vibrational relaxation mechanism for the fast time decay τ_1 and ET associated with τ_2. Vibrational relaxation effects on spectroscopy and kinetics have been studied for photodissociation of metal carbonyls, where the dissociation leaves large amounts of excess energy in low-frequency vibrations coupled to the CO stretching motions.[19,22] These studies show broad infrared absorption with line narrowing over time in the spectroscopic plots, and complex kinetics that can be biphasic. In these cases there are thousands of wavenumbers of excess energy in low-frequency vibrations, which have VR time scales in the $10-100$ ps range. In a kinetic model where the low-frequency VR is the shorter decay, one expects the $\nu' = 0$ level to have the simplest biphasic kinetics with a short decay equal to a rise time for the longer decaying component. For our kinetic traces near $\nu' = 0$ we are unable to fit the curves with a rise time of the 5 ps component equal to the decay time of the ultrafast component. This is also consistent with the presence of little internal energy in low-frequency modes at pump wavelengths of 800 and 700 nm, which we discuss in more detail in section B2 that models the absorption spectrum.

The inadequacy of the vibrational relaxation model combined with the ion-pair recovery kinetics suggests that both τ_1 and τ_2 involve ET. However, another alternative hypothesis that does not require two geometries in the ion pair is an ultrafast (<75 fs) conformational change in the initial radical pair with $\sim$50% yield of a new radical pair having a different ET rate. We show in a later subsection that a fast motion other than small translation is unrealistic, and we therefore suggest that two geometries in the ion pair is the best hypothesis.

Theoretical calculations with ab initio density functional methods show that two different stable geometries are possible

for the ion pair.[10] One is either double or triple contact of the O atoms of V(CO)$_6{}^-$ with the top of the cyclopentadiene ring (Figure 4a) and the second is side interactions of the O atoms with the Cp(Cp)$_2{}^+$, where the O atoms lie situated in the cleft between the two Cp rings (Figure 4b). With these methods,[10] we obtained interaction potentials for the two geometries in a continuum solvent model and calculated a 900 cm^{-1} energy difference between them, with the side contact geometry being the more stable entity. The calculation accuracy is not known, but this energy difference requires an equilibrium constant of $\sim$90. Additional description of the interaction potential is given in section B2.

The theoretical prediction of two geometries suggests that the relative amounts of each species might be obtained from the relative amplitudes of τ_1 and τ_2. However, the relative amplitudes are very wavelength dependent since both the charge-transfer spectrum origin and extinction would be different for two different geometries. As section B2 shows, more sophisticated models can be used to test the hypothesis, but here we can roughly assess this idea from basic data. If we assume equivalent IR extinctions and average the relative amplitudes of τ_1 and τ_2 over all pump wavelengths, we find an average ratio of amplitudes as 75/20. This value provides a 270 cm^{-1} energy difference between the two possible geometries via the simple thermodynamic relationship

$$\Delta G = RT \ln K_{eq} \qquad (1)$$

where $K_{eq} = 75/20$. This estimate suggests that two geometries might be present in the ion-pair equilibrium.

Both theoretical and experimental evidence suggests that two geometries are possible. In the next full section, B2, we provide a detailed experimental discussion and model for the electronic absorption spectrum that supports the hypothesis of two geometries, but which is not a direct experimental proof.

IVR and VR Processes. Our data have information on both IVR and VR processes. One obvious IVR process is implicit in the observation of transient IR absorption by the V(CO)$_6$ radical in the $\nu' = 1$ quantum state. Population in the IR-active CO stretch must occur via ultrafast IVR because the Franck$-$Condon analysis from theory and resonance Raman data (see section B2) show that IR active (nontotally symmetric) vibrations are not excited in the absorption process. The experiments show a rise time of 75 fs for the $\nu' = 1$ state. Since the IR-active mode cannot instantaneously obtain vibrational energy from the excitation process, a rise time in the excited-state signal is a direct indicator of the IVR time. This suggests that the time for 1-quantum IVR must be faster than the laser response function of $\sim$75 fs. Theoretical models for V(CO)$_6$ predict the totally symmetric stretch to be $\sim$100 cm^{-1} greater in energy than the IR-active stretch, while experiments for the anion give 162 cm^{-1} as the difference. The $\sim$100 cm^{-1} energy gap is large enough that energy and momentum matching by solvent collisions is not efficient. Studies suggest that the density of states for solvent phonons in the 100 cm^{-1} regime is not large enough to provide energy matching with an ultrafast IVR rate.[23,24] Therefore, IVR probably occurs with energy and momentum matching by both low-frequency vibrations within the molecule and solvent collisions. The accessibility of low-frequency vibrations is enhanced by the geometric changes simultaneously occurring through the necessary Jahn$-$Teller distortion. The optical excitation changes the O_h anion geometry to a D_{3d} geometry in the V(CO)$_6$ radical, where the C$-$V$-$C axis changes by $\sim$5°.

With 800 and 700 nm pump wavelengths, no resolvable rise time is observed except for $\nu' = 2$. The population of this level must also occur by IVR, which suggests that the ~200 fs rise time is the IVR time for two quanta of the IR active vibration. The conversion of two quanta of the totally symmetric mode at ~2073 cm^{-1} into two quanta of the nontotally symmetric mode at 1973 cm^{-1} requires a 200 cm^{-1} phonon for vibrational energy conservation, as opposed to the 100 cm^{-1} phonon needed for a single quantum. The solvent phonon density of states at room temperature will preferentially select the 1-quantum process over the two quantum process due to the greater probability of lower-frequency phonons.[25] From prior work[23,24] it is probable that conversion of two quanta of totally symmetric vibration into two quanta of IR-active vibration occurs by a consecutive process rather than a simultaneous change.

It should be noted that a Raman-active E_g mode exists for the radical that is very similar in energy to the IR-active mode. Though not observed experimentally, we estimate it to lie at ~1965 cm^{-1} based both on calculations and on the observed frequencies for other modes. It is possible that the totally symmetric stretch transfers vibrational energy to the E_g mode along with the IR-active mode through IVR processes. Previous transient absorption studies of vibrationally excited W(CO)$_6$ in the ground state[26] have shown how the 1980 cm^{-1} IR-active T_{1u} stretch can transfer energy to the Raman-active 2012 cm^{-1} E_g mode on a 10−20 ps time scale. However, energy was not transferred to the totally symmetric A_{1g} stretch at 2116 cm^{-1}. The IVR to the A_{1g} mode was proposed to be very slow compared to IVR to the E_g mode because it lies significantly higher in energy, thus making it more difficult for a solvent phonon mode to provide the necessary energy matching. In our case, the V(CO)$_6$ radical is undergoing a dynamic Jahn−Teller geometry change on the same time scale as the IVR, which could change the mechanism for IVR between the A_{1g} and E_g modes. If IVR were to occur first to the E_g modes and then to the IR modes, there might be evidence of a rise time in the IR absorption at all probe colors, which is not observed in the experiments. Therefore, if the E_g mode is involved three options exist: (1) the IVR conversion from the E_g mode to the IR mode is too fast to resolve, (2) the IR mode undergoes IVR to the E_g mode on a time scale that is longer than the back-ET rate of ~5 ps, (3) the totally symmetric mode initially distributes energy very quickly to both, establishing an equilibrium. The third of these hypothesis is unlikely since we see significant population in $\nu' = 2$, which would require significant population in higher quantum numbers from optical pumping if energy is to be shared with the E_g mode and IR mode. At 800 nm, the optical FCF's are inconsistent with pumping the radical to higher quanta than $\nu' = 2$ in any significant amount (see later discussion on FCF's), so this excludes the equilibrium concept. Therefore, the E_g mode is either part of an ultrafast IVR path that we cannot resolve or the IR mode decays into this mode on a time scale longer than 5 ps.

The VR process for high-frequency CO vibrations is expected to be quite slow (~100 ps) by analogy with ground-state studies of VR in related metal carbonyls[24,26] that also have a large difference in energy between CO frequencies and the next highest frequencies. The decay times of the $\nu' = 1, 2$ states imply a lower limit for the vibrational relaxation rate. For example, since the τ_2 decay time is 5 ps this implies that the VR relaxation time is greater than or equal to this value. The 5 ps decay has been shown to be consistent with ion-pair recovery rates here and in earlier work[8] and is essentially constant for all quantum levels. Therefore, only a minor part of this decay

can be from a competing VR channel in the upper quantum levels, and the VR time must be >5 ps.

The VR time for small populations of low-frequency vibrations is about 200 fs, as inferred from an observed rise time with 620 and 555 nm excitation wavelengths. This is discussed in the next subsection on geometric interconversion of the Jahn−Teller distorted radical.

In summary, the V(CO)$_6$ radical is initially populated with totally symmetric CO stretching vibrations that convert one quantum of IR-active stretch vibration by IVR in <75 fs. An ultrafast conversion by IVR also has been inferred for different inorganic complexes,[27,28] but the mechanism there may involve other electronic states. In our case, the mechanism appears to involve solvent collisions and low-frequency internal vibrations associated with a geometry change from an initial octahedral geometry of V(CO)$_6^-$ in the ion pair to a Jahn−Teller distorted geometry in the V(CO)$_6$ radical. It requires ~200 fs for conversion of 2 quanta of the totally symmetric CO stretching vibration into 2 quanta of IR-active CO vibration. The lifetime of the CO stretching mode in higher quantum states is not affected by VR, only by ET kinetics.

Geometric Interconversion of Jahn−Teller Distorted States. The experiments showed an unusual result where all vibrational states gave a rise time of ~200 fs in the ET rate once the excitation wavelength was decreased to 620 and 555 nm. This is unusual because with good FCF's for level $\nu' = 0$ in optical pumping (see section B2) this state is immediately accessible to transient absorption in the IR-active mode and does not require IVR from totally symmetric vibrations. Therefore, a significant population should be instantaneously created at all pump wavelengths, and there should not be a rise time of ~200 fs.

Our spectral modeling in the next section (B2) demonstrates that excess low-frequency vibrational energy exists in the excited state at shorter wavelength excitation. From this section we find that the fitted E_{00} value is 12 530 cm^{-1} for the dominant τ_1 ET rate component and that λ_s is 3020 cm^{-1}. Adding these values gives 15 550 cm^{-1}, the energy of typical $0 \rightarrow 0$ vibronic transitions. Pump wavelengths of 620 and 555 nm exceed the $0 \rightarrow 0$ transition energy by ~600 and 2500 cm^{-1} respectively, placing excess vibrational energy in the radical pair. Of course, the spectral inhomogeneity implies that there is a distribution of molecular environments and bond distances, so that a 700 nm excitation wavelength still has some probability of leaving excess internal energy in the molecule. From our least-squares fitting to the kinetics, we estimate that a ~200 fs rise time component could contribute 15% of the total signal at 800 and 700 nm and not be resolved from the dominant instantaneous component. This implies that the sudden dominance of a rise time at 620 and 555 nm is a major change from the transients observed at longer excitation wavelengths.

Prior theoretical modeling has shown that after excitation, the radical geometry relaxes from nearly O_h symmetry to a D_{3d} geometry[10] due to the Jahn−Teller effect. However, this work also found a D_{2h} geometry only 207 cm^{-1} higher in energy than the D_{3d} geometry with a single imaginary frequency demonstrating its instability to vibrational distortion. There could also be other geometric structures that exist close in energy to these computed structures, so that with excess vibrational energy the radical geometry may be undergoing interconversion between several symmetries. Such interconversion on <200 fs time scales will not provide a definitive frequency for the CO stretch, and any IR absorption would have lifetime broadening and an extinction below our noise levels until a distinct geometry is

recovered by VR of low-frequency vibrations to the solvent. Therefore, in this model the absorption rise time is the VR time required to reach the lowest energy geometry where a well-defined absorption exists for $\nu' = 0$, 1, and 2. A coalescence effect has been observed previously for carbonyl stretches in organometallic systems exhibiting rapid intramolecular ET and two structures.[29-31] In our case absorption becomes apparent with a 200 fs rise time as the system relaxes to the well-defined D_{3d} geometry from interconversion between many geometries. The theoretical calculations indicate that the CO frequencies for the D_{3d} and D_{2h} symmetries lie within 10 cm^{-1}, which is probably similar for all geometries, and therefore the spectral peaks should not produce a very broad band. However, on a 200 fs or shorter time scale, this band would be lifetime broadened to be $\geq$170 cm^{-1} fwhm. In this scenario, the extinction would be spread over a wide frequency range and would not be observable with our level of noise. A spectrum of the excited-state carbonyl region over the frequency range 1921–2041 cm^{-1} was acquired 100 fs after excitation for a 620 nm pump and it confirms a broad region with little transient absorption outside of the expected wavelengths.

A conjecture that is inconsistent with the data would involve a higher-energy electronic state becoming accessible at 620 nm. In this case we would not require the IR mode to become observable immediately but would require a relaxation time to a lower-energy electronic state. This putative upper state would also have charge-transfer character to create the radicals, and therefore it would also have broad electronic absorption widths and similar vibrational frequencies to a lower state (also, with lifetime broadening during any electronic relaxation). However, broad electronic absorption implies that there cannot be such sudden access at 620 nm to another electronic state, and we would therefore expect to excite some population to a higher-energy state at 700 and 800 nm, leading to a rise time component at every pump wavelength.

In summary, the onset of a rise time for all transient IR absorptions at 620 and 555 nm suggests a new mechanism is occurring in the radical pair to increase the rise time above the resolution limit of 75 fs. We have shown from the spectral modeling that these wavelengths have a small amount of internal energy in low-frequency vibrations that is sufficient to excite interconversion between different Jahn–Teller structures. The rise time then results from VR of low-frequency vibrations to the solvent in 200 fs, allowing V(CO)$_6$ stabilization into the lowest Jahn–Teller geometry.

Motion in the Radical Pair. A mechanism for an ultrafast component of decay that invokes ultrafast creation of a new conformation in the radical pair is unlikely. The <75 fs rise time at 800 and 700 nm excitation for $\nu' = 0$ and 1 suggests that any motion leading to a new conformation would need to be very fast while also having ~50% conversion to create two species with different ET rates. Since the ET rates are quite different, a new conformation requires significantly different coupling, which would not result from the simple case of small translational motion. We might conjecture that excess internal energy would promote motions such as rotation of the V(CO)$_6$ radical. For example, in a geometry such as the side-bonded case in Figure 4b a 180° rotation would give very different interaction matrix elements. We show in later sections that 800 and 700 nm pump wavelengths provide little excess vibrational energy in the radical pair, but we do expect 620 and 555 nm pump wavelengths to provide enough excess energy to possibly increase the yield of any rotated component. Indeed, at these wavelengths the data of Table 1 show that the amplitude of the

faster ET component τ_1 increases relative to the slower component τ_2, which is consistent with the argument for motion, and indirectly assigns the faster component to the rotated species. Furthermore, in this hypothesis the rotated species cannot be thermally accessible from the starting geometry since it has the larger ET rate and would deplete the 5 ps component; therefore the rotated species only would be correlated with internal energy created by optical excitation. We can estimate the time for rotation of the V(CO)$_6$ radical by assuming a free rotor model. From Gaussian 98W[32] calculations of geometry, we obtain a rotational constant about one axis of 0.607 GHz for the radical. This value equals $h/8\pi^2 I$, where h is Planck's constant and I is the moment of inertia about the axis. By assuming $^1/_2$ k_BT of energy in a classical rotor about one axis and $T = 298$ K, we calculate a time of 11.5 ps per full revolution of the radical, or 64 fs to rotate 2 degrees. Therefore, for a <75 fs rise time we conclude that thermal rotation of the radical is negligible and that relative motion of the two radicals would require an unrealistically large amount of internal rotational energy to change the orientation on this time scale.

B2. Models For the Absorption Spectrum of Two Geometries. Analyzing a broad absorption spectrum to infer the existence of two geometries is problematic when there is no direct measurement of two species by another technique. However, we can use both theoretical models and kinetic data to check for consistency of the hypothesis. The following subsections discuss different elements of the analysis, but the main outcome is that a model with two geometries is more satisfactory than a model with a single geometry. However, even though the models in this section are required to give confidence in the hypothesis of two geometries, the results are not sufficient to be a proof. This section is necessarily complex, and is not required for those readers interested in the trends of ET rates discussed in the next section C.

The first subsection examines the absorption spectra versus temperature to demonstrate the difficulty of separating the spectral contributions. The second subsection uses populations in quantum levels from transient kinetics experiments to provide FCF's for the optical absorption and compares these with theory. The third subsection uses resonance Raman analysis and FCF analysis to decompose the absorption spectrum and compare the fit for a single geometry versus two geometries that have offset origins. This provides the best evidence for two geometries. The fourth subsection compares experimental observations of ET component intensity and quantum populations versus excitation wavelengths as an additional test of the two-geometry hypothesis. A fifth subsection is a short summary, where we conclude that two geometries are possible for the ion pair.

This study of the absorption spectra reveals two issues that require further theory and experiment. The first is that a better analysis could be done with new theoretical tools for treating asymmetry of the inhomogeneous broadening. The second is that the experimental data may have distortion of the initial quantum populations because of ultrafast ET and re-excitation of ground state vibrationally excited species during the optical pump pulse.

Absorption Spectra versus Temperature. Since the equilibrium constant in eq 1 is temperature-dependent, low-temperature absorption spectra were obtained for the ion pair to examine whether an asymmetric change in the absorption band would occur as the equilibrium constant changes with temperature. Spectra are displayed in Figure 5 that were obtained from 296 to 173 K in ~20 K increments. The absorption maximum blue shifts from 16 130 cm^{-1} to 18 050 cm^{-1} and intensifies as the
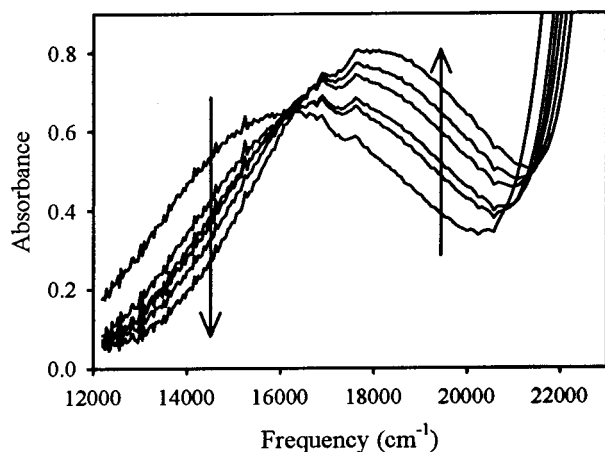
Figure 5. Temperature-dependent charge-transfer absorption spectra for the [Co(Cp)$_2$$^+$|V(CO)$_6$$^-$] ion pair in dichloromethane. Arrows indicate the growth/decrease of the absorption spectrum as the temperature is cooled from 296 to 173 K in ~20 K increments.

temperature is lowered. The bandwidth change cannot be precisely determined due to the presence of a large-intensity absorption with an onset at ~22 000 cm^{-1}. The blue shift is due to an increase in the solvent dielectric constant as the temperature is lowered. We fit the band shapes with an inhomogeneously broadened line and find that very little change in band shape is present while a slight narrowing (~1000 cm^{-1}) occurs over the temperature range. The interpretation of this result relies on expectations for the temperature dependence of the free energy. The following argument indicates that temperature shifts in two equilibria are more difficult to identify than a simple shift of one equilibrium, and therefore the lack of temperature effects on band shape is not definitive over such a limited temperature change.

The two putative geometries each exist in an ion-pairing equilibrium, where

$$\text{I}_1 + \text{I}_2 \overset{K_\text{d}}{\rightleftharpoons} \text{IP}_\text{d} \tag{2}$$

and

$$\text{I}_1 + \text{I}_2 \overset{K_\text{t}}{\rightleftharpoons} \text{IP}_\text{t} \tag{3}$$

with IP$_\text{d}$ and IP$_\text{t}$ respectively representing the concentrations of the ion-pair double and triple contact geometries and I$_1$ and I$_2$ representing the Co(Cp)$_2$$^+$ and V(CO)$_6$$^-$ ion concentrations. The relative concentrations of the two ion-pair species is proportional to the equilibrium constants K_d and K_t

$$\frac{K_\text{d}}{K_\text{t}} = \frac{\text{IP}_\text{d}}{\text{IP}_\text{t}} \tag{4}$$

Taking the natural logarithm of both sides of eq 4 and simplifying, we obtain

$$\ln K_\text{d} - \ln K_\text{t} = \ln \text{IP}_\text{d} - \ln \text{IP}_\text{t} \tag{5}$$

We multiply by $-RT$

$$-RT(\ln K_\text{d} - \ln K_\text{t}) = -RT(\ln \text{IP}_\text{d} - \ln \text{IP}_\text{t}) \tag{6}$$

and substitute into eq 1 to give

$$(\Delta G_\text{d} - \Delta G_\text{t})/T = -R(\ln \text{IP}_\text{d} - \ln \text{IP}_\text{t}) \tag{7}$$

This expression demonstrates that a difference in free energy must change with temperature to show temperature effects on concentration. The Gibbs–Helmholtz equation

$$\frac{\partial}{\partial T}\left[\frac{\Delta G}{T_\text{P}}\right] = -\frac{\Delta H}{T^2} \tag{8}$$

shows that the left-hand side of eq 7 will change according to ΔH differences, which are likely to be temperature insensitive individually and even less sensitive as a difference. Therefore, we expect little temperature effect on the relative concentration changes that could asymmetrically affect the absorption spectrum.

Franck–Condon Factors from Kinetics and Theory. It is possible to use the relative populations prepared in each vibrational quantum of the IR-active symmetric CO stretch to estimate the Franck–Condon factors for the totally symmetric CO stretch mode. The relative populations in each quantum level can be inferred from the values reported in Table 2, and we use the absorbance values obtained at 800 nm since this pump wavelength is the least susceptible to the effects of re-exciting the sample (see later section). At 800 nm, the relative signal intensities scale as 0.40, 0.33, and 0.27 for levels $v' = 0$, 1, and 2. Since we are examining a multilevel system, the signal intensities do not probe the actual level populations, but rather the population differences between adjacent levels. Therefore, the observed signal intensities are due to relative populations of 1.00, 0.60, and 0.27. We have done some modeling of how multilevel absorption affects the kinetics and absorption intensities, and fortunately more sophisticated modeling makes slight difference for our particular rate parameters. The initial absorption into totally symmetric CO stretching modes and conversion into IR-active modes by ultrafast IVR was discussed in a prior section. Since we identified no population loss processes other than ET in the kinetics for 800 and 700 nm excitations, it is possible to equate the relative populations to the absorption process and infer relative Franck–Condon factors (FCF's) for the totally symmetric CO stretching mode in V(CO)$_6$$^-$. We obtain values of 0.53, 0.32, and 0.13 for the 0 → 0, 0 → 1, and 0 → 2 vibronic transitions in the totally symmetric CO stretching vibration.

The FCF's can be used to estimate the dimensionless mode displacement (Δ). Following standard procedures for modes with displacements and no frequency changes,[13,14] the FCF's for each final quantum state n can be obtained via

$$\text{FCF} = e^{-S}\frac{S^n}{n!} \tag{9}$$

where S is the Huang–Rhys factor with $S = \Delta^2/2$. The Δ value dictates the FCF distribution, and we find the smallest discrepancy between the calculated FCF's and our data for $\Delta = 1.15$, where the relative FCF's for vibronic transitions 0 → 0, 0 → 1, and 0 → 2 equal 0.53, 0.35, and 0.12, respectively. This displacement lies very close to the $\Delta = 1.21$ value previously calculated for the totally symmetric stretch occurring at 2020 cm^{-1}.[10] This experimental method of estimating FCF's from populations at one wavelength is not rigorously correct for a broad spectrum with large line broadening. The following section predicts populations as a function of wavelength to check for consistency of these particular FCF's with the spectra and with the quantum resolved populations. This effort suggests that the FCF for the transition 0 → 2 is probably too large, possibly from repumping of vibrationally hot ground states. The next section also suggests deficiencies with symmetric line broadening models.

Electronic Absorption Spectral Analysis. The analysis objective is to demonstrate that the absorption spectrum predicted by assuming a single ion pair is less consistent with the experimental and theoretical FCF's than a model of two ion-pair geometries. The method initially uses a technique from resonance Raman analysis that links FCF's and absorption spectra with a model for line broadening effects. One test of the model is to compare predictions of component populations at each excitation wavelength to experiment.

The details of time-dependent resonance Raman analysis and its relation to the electronic absorption spectrum are beyond the scope of this manuscript, and we refer the reader elsewhere for an introduction.[33−41] The main goal of the Raman analysis is to extract mode displacements for the totally symmetric vibrations that contribute to the absorption spectrum and Raman spectrum. The mode displacements can in turn be used for computing the absorption FCF's.

Resonance Raman data for the ion pair have been analyzed and reported previously.[10] Here, we reexamine the data with formerly unavailable software generously provided to us by the laboratory of Anne Myers Kelly of Kansas State University. To test the assumption of a single absorption band, the lifetime broadening was fixed at a typical value of 20 cm^{-1} and the solvent reorganization energy was fixed at 3020 cm^{-1}, where the value is obtained from isodensity polarized continuum (IPCM) calculations of solvation energy for both ion pairs and radical pairs that were modeled by density functional calculations.[10] In the resonance Raman software, the solvent reorganization is incorporated as a Brownian oscillator model.[42−44] The fit to the absorption spectrum iterated the inhomogeneous line broadening and relative mode displacements of the observed resonant modes while maintaining their relative scattering intensities. We again took into account three additional totally symmetric modes not experimentally observed but calculated to have small displacements. These modes have been discussed in prior publications, and their displacements were fixed based on geometry calculations for the V(CO)$_6^-$ and V(CO)$_6$ species.[10] Our results give an E_{00} value of 12 740 cm^{-1} and a large inhomogeneous line width of 1820 cm^{-1}, where the large inhomogeneous width is necessary to fit the low energy tail of the absorption band. Some inhomogeneity is expected (see later discussion) due to the small interaction energy of the ion pair and resultant variation in ion−ion distance. The fit gives a dimensionless displacement of $\Delta = 0.81$ for the totally symmetric CO stretching mode, which is much smaller than the theoretical value of 1.21. From the fitted displacement we can compute FCF's for the $0 \rightarrow 0$, $0 \rightarrow 1$, and $0 \rightarrow 2$ vibronic transitions as 0.72, 0.27, and 0.05, respectively. From the prior section we derived experimental estimates of these FCF's as 0.53, 0.35, and 0.12, which suggests an inconsistency between the modeled spectrum and experiment. We are not able to adjust the relative displacements to bridge such a large difference while still maintaining a satisfactory fit to the absorption spectrum, and we conclude that a second ion-pair species might be present.

The model of two geometries, with offset charge-transfer absorptions can be developed similar to the single geometry model. The mode displacements were assumed to be identical for both spectra and to differ only in their absorption origin (E_{00}) and intensity. The displacement of the 2020 cm^{-1} totally symmetric mode was held fixed at $\Delta = 1.15$, which is from the experimental populations (and similar to theoretical calculation). We iterated the remaining mode displacements as described above to fit the spectrum. Initial estimates of E_{00} and the inhomogeneous line width were assigned and then the

TABLE 3: Parameters Obtained from a Time-Dependent Raman Analysis of the Resonantly Enhanced Vibrations[a]

mode frequency (cm^{-1})	Δ	Δq (Å)	λ_{vib} (cm^{-1})
84*	0.50		10
315	1.28	0.037	258
373	0.86	0.028	138
1114*	0.10		6
2020	1.15	0.017	1336
3100*	0.01		<1

[a] We show dimensionless displacements (Δ), coordinate displacements (Δq), and vibrational reorganization energy (λ_{vib}) for the resonantly enhanced modes. Modes with an asterisk were not experimentally observed, and their values for Δ are predicted from calculation.
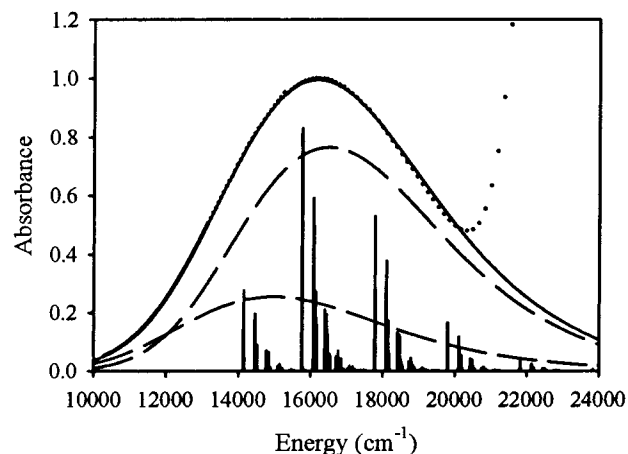

Figure 6. Experimental absorption spectrum for the ion pair in dichloromethane (dotted line), sum of proposed absorptions to fit the total experimental spectrum (solid line), fits to proposed individual absorptions obtained from time-dependent resonance Raman analysis (dashed lines), and vibronic progressions calculated from Franck−Condon factors.

TABLE 4: Observed and Calculated Amplitude Ratio of ET Components τ_1 and τ_2 for $v' = 0$

pump wavelength (nm)	τ_1/τ_2 amplitude ratio	
	obsd	calcd
800	1.5	1.4
700	1.1	2.3
620	2.7	3.2
555	4.2	4.0

absorption origins of the two bands and inhomogeneous line width were also iterated while maintaining a τ_1/τ_2 amplitude ratio that correlated with that observed experimentally for $v' = 0$. We obtained E_{00} values of 12 530 ± 175 cm^{-1} and 11 280 ± 175 cm^{-1} for the two bands with relative peak amplitudes of 0.75 and 0.25, respectively, where ET component τ_1 correlates with the higher-amplitude band and higher-energy absorption origin. We obtained a large inhomogeneous line width of 1525 ± 75 cm^{-1}, which is smaller than that required for a single band model. Similar to prior results, the large value for inhomogeneity is necessary to fit the low-energy tail of the absorption band.

Calculated dimensionless mode displacements, bond length displacements (Δq) and vibrational reorganization energies (λ_{vib}) for the resonantly enhanced modes are reported in Table 3. Figure 6 displays the experimental absorption spectrum and the two-band fit obtained with the Raman software. Table 4 has the fitted and experimental τ_1/τ_2 amplitude ratios (from Table 1) for $v' = 0$ at each pump wavelength. Reasonable correlation is seen in the relative amplitudes of the two spectra at all pump
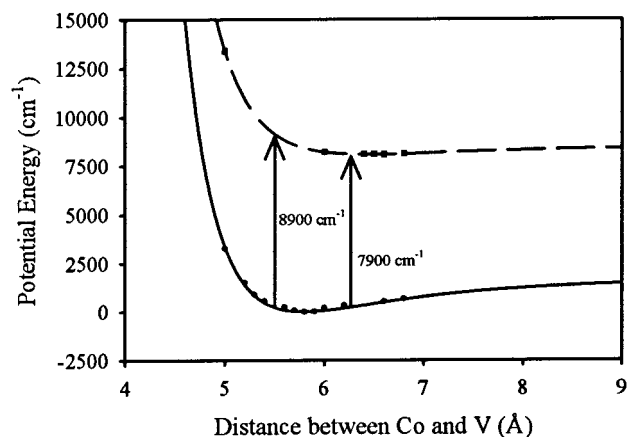
1162 *J. Phys. Chem. A, Vol. 106, No. 7, 2002*

Marin et al.

Figure 7. Calculation of interaction potential versus metal separation distance for the $[Co(Cp)_2^+|V(CO)_6^-]$ ion pair (solid line, circles) and $[Co(Cp)_2|V(CO)_6]$ radical pair (dashed line, squares) assuming the more stable side contact geometry. Results indicate possible transition energies ranging from 7900 to 8900 cm^{-1} at room temperature, which implies substantial inhomogeneous line broadening.

TABLE 5: Relative Populations in Vibrational Quanta Predicted To Be Excited in the $[Co(Cp)_2|V(CO)_6]$ Radical Pair with Various Pump Frequencies[a]

ET rate component	pump wavelength (nm)	rel population in vibrational quanta			
		$v' = 0$	$v' = 1$	$v' = 2$	$v' = 3$
τ_1	800	0.92	0.08	-	
	700	0.81	0.18	0.01	
	620	0.63	0.34	0.03	
	555	0.43	0.45	0.13	
τ_2	800	0.83	0.17	0.03	
	700	0.66	0.30	0.04	
	620	0.46	0.44	0.09	
	555	0.33	0.44	0.20	0.03

[a] Relative values are normalized to unity at each pump wavelength and for each component.

wavelengths except 700 nm, so the basic trend duplicates the domination of component τ_1 at shorter excitation wavelengths. The deviation at 700 nm could be due to experimental error since the $v' = 1$ case has a predicted τ_1/τ_2 amplitude ratio of 1.7, which is in better agreement with the trend over all the wavelengths. This comparison in Table 4 is the best demonstration of how offset spectra yield relative intensity changes in the components, and it supports the hypothesis of two ion-pair geometries rather than a single geometry. The agreement of any two geometry model will be better than a single geometry model, even if a inhomogeneous line broadening model was available that included asymmetry of the broadening.

Relative Quantum Populations versus Excitation Wavelength. Since the experimental data are resolved by quantum number, it is possible to do further spectral decomposition to model individual quantum contributions. This level of detailed comparison is useful to demonstrate the theoretical method, but is not as successful in testing the two geometry model as was the previous section. However, the method does reveal a need for new theoretical tools in treating spectral inhomogeneity, and it also suggests a probable problem in our experimental populations for large quantum numbers.

The conversion of mode displacements to FCF's for specific combination bands can be used to generate a spectrum for all transitions involving the totally symmetric mode. We have adapted software designed for multidimensional FCF computations[45] for this simpler simulation problem. The simulation gives the numerical FCF values for every combination band within the vibronic progression of the electronic absorption band. It can therefore generate a "gas phase" stick spectrum, which is shown in Figure 6. The 2020 cm^{-1} mode dominates the progression due to its high λ_{vib} value, causing it to carry ~75% of the total vibrational reorganization energy.

The large inhomogeneity is probably due to the relatively small interaction energy in the ion pair causing a greater range of stable distances between the ions. A plot of the calculated interaction potential between the Co and V atoms versus distance is shown in Figure 7, where we assumed the more stable side contact geometry for both the ion pair and radical pair. This figure has added more points to the work reported previously.[10] The potential wells are shallow, and calculations indicate that at room temperature ($k_B T = 207$ cm^{-1}) a distance range of 5.5–6.2 Å exists between the metal centers, giving transition energies

ranging from 7900 to 8900 cm^{-1}. This broad range of transition energies is the probable source of the inhomogeneous line broadening. However, this also implies that the assumption of a symmetric inhomogeneous line width is likely incorrect. A model creating an asymmetric line width from the fitted potential curves in Figure 7 would likely improve the fitting quality, and it is a subject for future research. The expected effects of a variable distance on the ET rate can be estimated from the charge-transfer absorption formula of Hush.[9] The coupling matrix element is inversely proportional to distance and the rate squares this value so that a range of 0.7 Å out of 5.85 Å gives a 25% rate variation. This variation is too small to explain the two components of ET rate, but does give some small distance variation in the measured rates.

We can now use the above information to predict the relative populations of vibrational quanta excited with a particular pump frequency. This is done by first generating an absorption spectrum with the Raman software that includes all other combination bands and broadening parameters, but with no change in the quantum number of the 2020 cm^{-1} progression. This reference spectrum is then displaced in energy by $v \times 2020$ cm^{-1} ($v = 1, 2, ...$) and each displaced spectrum is amplitude weighted by the FCF's of the 2020 cm^{-1} mode so that the sum generates the full absorption spectrum for the geometry. It is then possible to estimate how many quanta of the totally symmetric mode are excited at any excitation frequency by simply checking the value of each individual spectrum underneath the full spectrum at that frequency. Since the experimental spectrum is broad and featureless, there is no simpler way to estimate these values. The functional form for the reference spectrum is not analytic, but it can be adequately fit with the sum of two Gaussian functions and then shifted and weighted as indicated for all other quanta. At any pump frequency, we can compute the relative amounts excited into each quantum level by the amplitudes of each spectral component.

The values indicating the relative populations in a particular quantum level are reported for our excitation frequencies in Table 5 for the two spectra associated with τ_1 and τ_2, and Figure 8 plots the absorption spectrum for ET component τ_1 fit as described above. The normalization in Table 5 that illustrates relative populations in different quantum levels is less useful for comparison to experiment, but the tabulated values show how shorter excitation wavelengths allow greater amounts of population into larger quantum numbers for both components. The predictions show the greatest population in $v' = 0$ at all of our excitation frequencies but 555 nm. At 800 and 700 nm, we should get very little population in $v' = 2$. At 555 nm, where we would expect the most population from $v' = 2$, we still only expect ~20% contribution to the total amount pumped. These
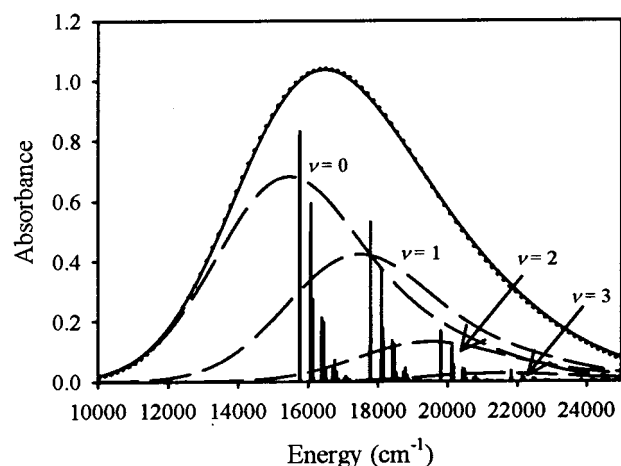
Figure 8. Illustration of how individual spectra assigned as subsets of the 2020 cm^{-1} totally symmetric progression (dashed lines) can be summed to give the total absorption spectrum (solid line). The value of each of these "subspectra" at a given frequency provides relative amounts of the vibrational quanta excited at that frequency. The amplitudes of the subspectra scale according to the FCF's of the 2020 cm^{-1} progression.

TABLE 6: Relative Transient Absorbance Intensities for the [Co(Cp)$_2$|V(CO)$_6$] Radical Pair and the Expected Relative Intensities Inferred from the Spectral Analysis by Subtracting Populations^a

ET rate component	pump wavelength (nm)	rel signal intensities			expected rel signal intensities		
		$v'=0$	$v'=1$	$v'=2$	$v'=0$	$v'=1$	$v'=2$
τ_1	800	0.21	0.22	0.27	0.53	0.05	
	700	0.25	0.20	0.18	0.54	0.15	0.01
	620	0.27	0.27	0.30	0.35	0.37	0.04
	555	0.25	0.41	0.23	0.03	0.55	0.23
τ_2	800	0.14	0.13	0.03	0.33	0.07	0.02
	700	0.23	0.12	0.03	0.17	0.12	0.02
	620	0.10	0.06	0.01	0.01	0.18	0.05
	555	0.05	0.05	<0.01	0.04	0.09	0.06

^{a} Relative signal intensities at each pump wavelength are normalized so that values for $\tau_1 + \tau_2$ sum to unity.

discrepancies suggest that too much population is in $v' = 2$, which might be partially resolved by a new model of asymmetric inhomogeneous broadening. In the next paragraphs we make the predictions more explicit and use this to comment on probable deficiencies in the data due to re-excitation processes during the pump pulse.

The expected relative signal intensities due to the differences in population between adjacent levels are shown in Table 6 along with the observed relative signal intensities. Relative signal intensities at each pump wavelength are normalized so that values for $\tau_1 + \tau_2$ sum to unity. This normalization gives a better sense of relative signals for each component at a particular wavelength. Since these predictions use a difference of the numbers reported in Table 5, which are based on only an approximate model, we can only expect an approximate correspondence to experiment. The agreement is not good, and the observed signal intensities suggest that much more population is excited to higher quantum levels than predicted from the absorption model. This deviation would be even worse for a model with one ion-pair geometry.

A possible reason for the large signals in $v' = 2$ is that a small amount of the ground-state population is likely being re-excited from vibrationally hot ground-state levels, causing excess population in higher excited-state levels. The lifetime resolution of about 75 fs implies that we cannot check if the ET rates

during the pump pulse(see later discussion) are larger than inferred at longer times. Therefore, accurate determination of the population that can be re-excited within the duration of the pump pulse is very difficult. Even with the observed ET rates, we estimate that up to 15% of the excited population for component τ_1 might return to the ground state within the duration of the pump pulse. After returning to the ground state, some fraction of the population will lie in $v = 1$ and 2, and molecules having these hot vibrations can be re-excited to increase populations in higher quantum numbers for the radical. Since $\Delta v = 0$ and 1 have the best FCF's, we expect enhanced excitation to levels $v' = 1$, 2, and 3. Thus, any re-pumping should cause additional population in $v' = 1$ and 2, thereby causing greater transient absorption for $v' = 1$ and 2. This hypothesis could be tested with a power dependence study, as more pump power should enable more of the sample to be re-excited. Unfortunately, our signal-to-noise ratio is not high enough to be able to test this over the required range of pump powers. In the next section we discuss prior data on this system where pulses of 2−3 ps duration required a second pulse to create significant population in $v' = 2$, which is support for the idea of re-pumping in the current experiments. Though re-excitation of the ground-state population helps explain the discrepancies between the expected and observed signal intensities, its magnitude depends critically on the ET kinetics at times <75 fs. If there is significant ET on this time scale due to heterogeneous rates, then re-excitation could have a larger effect.

In conclusion, our predictions of the experimental transient absorption intensities as a function of quantum level do not agree well with the experiment for larger quantum numbers and for the red edge of the spectrum at 800 nm. The model would agree less well with a single geometry for the ion pair, so the major outcome of this more detailed analysis is to provide insights into possible problems with the method. For example, such a detailed spectral model must be more sophisticated to account for asymmetry in the inhomogeneous broadening, where asymmetry on the red side of the spectrum could greatly affect our predictions at 800 nm. In addition, the model cannot explain the observed strong signals for $v' = 2$, which we interpret as support for ion-pair vibrations being re-excited during the pump pulse.

Summary. The absorption spectrum is most consistent with two ion-pair geometries having absorption origins different by about 1250 ± 350 cm^{-1}. We assign the band at 12 530 cm^{-1} to ET component τ_1 and the band at 11 280 cm^{-1} to ET component τ_2. The assignment roughly predicts the trend in relative amounts of each component as a function of excitation wavelength, but it less successful in correlating quantum populations with excitation wavelength. The shift in absorption band origin of the two spectra does not allow computation of the free energy differences of the two structures because of the unknown extinction in the charge-transfer band.

The procedure for modeling the quantum dependence of transient absorption intensities is only approximate since asymmetry of the inhomogeneous broadening was not used in the spectral modeling. Such a model might be derived from the ion-pair and radical-pair potential energies, and this is a subject for future work. The deviations between the model and the experiment in explaining the observed strong signals for $v' = 2$ suggests that there may be some re-excitation of ground-state levels during the pump pulse.

The spectral modeling developed in this section only provides an estimate for the charge-transfer absorptions of two ion-pair geometries. This is not sufficient to unequivocally prove the

1164 *J. Phys. Chem. A, Vol. 106, No. 7, 2002*

Marin et al.

two geometry hypothesis or assign the spectral splitting. The two geometry hypothesis ultimately has its origin in the experimental observation of biphasic ET kinetics, which is difficult to understand with any other mechanism.

C. Electron-Transfer Rates. *Nonequilibrium Electron Transfer.* The prior sections have shown that many complex phenomena can be occurring in the radical pair immediately after excitation. The types of nonequilibrium phenomena that can affect electronic overlap and ET include structural effects such as the Jahn−Teller geometric interconversion and motional effects in the radical-pair distance that arise from heterogeneity in the initial ion-pair contact distance. Additional nonequilibrium effects arise from solvent reorganization on the time scale of the longitudinal relaxation time, τ_L. These solvent effects have been discussed for ET processes,[46] and for dichloromethane the calculated τ_L time is 330 fs while the measured time is ∼400 fs for dye molecule probes.[46−48] The apparent ET rate of 400−700 fs is on the same time frame as τ_L, and there might be some nonexponential character in the ET time decay. However, the solvent effects are not well understood in this particular time regime.[7,27,28]

There is little change in vibrational population of the IR-active CO stretching mode after the first 75 fs, where populations are becoming stabilized via IVR. The ET process during the first 75 fs is not well defined due to the dynamic effects of IVR and geometry change, and is in the nonequilibrium regime. In addition, when small amounts of excess vibrational energy exist in the lower-frequency vibrations, we have inferred a Jahn−Teller geometric interconversion relaxation time of ∼200 fs, the time for VR in the low-frequency modes. This interconversion kinetics also provides some nonequilibrium ET component for excitation wavelengths of 620 and 555 nm. All of these nonequilibrium aspects of ET are not fully understood, and therefore making conclusions about ET rates versus quantum state require additional consideration of the experimental time scales and wavelengths where they will be minimal. From the prior sections it appears that for 800 and 700 nm excitation many of the nonequilibrium effects are minimal for times >75 fs.

Quantum Dependence of Rate. A quantum dependence of the τ_1 ET rate is observable for all pump wavelengths, where 800 and 700 nm excitation shows an average 10% increase from $\nu' = 0$ to $\nu' = 1$ and 45% increase from $\nu' = 1$ to $\nu' = 2$. This component is for a particular geometry, although we do not know which of the two candidates in Figure 4 correspond to the ultrafast component. Within our signal-to-noise levels, no quantum dependence is observable for τ_2 or τ_3, and this means that the ion-pair geometry leading to an ET time of ∼5 ps has no quantum dependence.

The standard models for calculating nonadiabatic ET rates are exclusively based on vibrational tunneling via totally symmetric modes.[13,14] These models cannot explain the observed quantum dependence in these experiments, where a nontotally symmetric vibration changes the ET rate. One explanation of this quantum effect, which we have proposed previously,[8,10,14,20] might be that the amount of electronic coupling could be dependent on vibrational quantum number via a breakdown of the Condon approximation, where a difference in electronic coupling exists for different vibrational quanta. Further studies of the matrix elements are required to demonstrate the validity this hypothesis.

Additional effects from Duschinsky mixing of vibrations have been recently investigated in our group to demonstrate the possibility of large ET rate effects in some molecules, but these will not provide quantum effects.[45,49] In particular, calculations have been done with the $V(CO)_6$ radical and ion to show that only moderate Duschinsky effects are likely for this molecule.[49]

It is unlikely that ultrafast VR and IVR processes contribute to quantum differences in the ET rates. We discussed these processes earlier in this manuscript and showed that IVR is complete in <75 fs, so it will not affect the rates for 800 and 700 nm excitation. We also showed that VR in the IR-active CO stretching vibration is on time scales >5 ps. While the 5 ps and 700 fs ET components are for two different ion-pair geometries, we expect that any VR in the $V(CO)_6$ radical should be similar for both geometries, which means that VR must be >5 ps and cannot be affecting the 700 fs rates. The nonequilibrium effects from Jahn−Teller interconversion appear to occur in the first 200 fs for 620 and 555 nm excitation wavelengths. Since additional nonequilibrium effects are present for excitation with 620 and 555 nm, it is likely that the 800 and 700 nm data better isolate quantum effects for the IR-active CO stretching mode.

We conclude that for the geometry exhibiting ∼700 fs ET there is a quantum effect with an increase of 10% for the first quantum above $\nu' = 0$ and an additional increase of 45% as the quantum level increases to $\nu' = 2$ from $\nu' = 1$. The increase in rate of 45% is too large to be easily explained by standard ET rate models for a nontotally symmetric mode, and we assign it as due to a breakdown of the Condon approximation.

Comparison to Prior Results. The data reported here seem contradictory to those previously reported from our laboratory,[8] but the explanation is due to the very different experimental time resolutions. Larger signals were seen formerly, where the change in absorbance was on the order of 0.2. The current data had ∼100 times smaller absorbance changes due to 100 times less pump laser energy per pulse. Less pump energy was necessary in the current experiments to prevent nonlinear optical effects within the sample and cell windows due to the high peak power of the ultrafast pulses. Previous experiments had difficulty in observing any signal for level $\nu' = 2$ without a second, delayed pump pulse, whereas for current experiments, no special arrangement was necessary. This indicates that our peak power is substantially higher than in previous experiments even with ∼100 times less energy per pulse. The shorter pump pulse enables more re-excitation of the ground-state population for ultrafast ET.

The ∼2−3 ps time resolution in previous experiments was too long to reveal the ultrafast ET component τ_1, which dominates the kinetics for every pump and probe combination in the current experiments. Prior experiments revealed a 2-fold rate increase for each quantum level, where here we only have a quantum effect in the ultrafast component of 10% and 45% for successive quanta. The rates previously were 26.4, 11.3, and 5.5 ps for $\nu' = 0$, 1, and 2, respectively, where a single exponential was used to fit the decays. We are able to use simulation to approximately show how the inability to resolve the presence of τ_1 leads to a quantum dependence of decay rate. In the original measurements, even though τ_1 could not be measured, a pulse width limited feature contributes to the intensity profile. Since the current data show that the *relative amplitude of τ_1 versus τ_2 increases with quantum number*, fitting a single exponential over the combined pulse width limited feature and 5 ps component gives a decay time that decreases substantially with quantum number. Component τ_3 was not used previously to fit the prior baseline recovery, and its omission probably lengthened the fitted decay times for the lowest quantum level. The combined effect of low time resolution and

Electron Transfer in [Co(Cp)₂|V(CO)₆]

J. Phys. Chem. A, Vol. 106, No. 7, 2002 **1165**

an increasing quantum yield at higher quantum levels for the unresolved ultrafast component is the main explanation why the prior data showed a quantum effect. The current data only show a quantum effect for an ultrafast component, not the longer 5 ps component.

In previous experiments, a rise time was observable in the ion-pair recovery on a time scale comparable to the relaxation of τ_2 in the excited state. This could correspond in part to the 5 ps component, but a faster rise time component was absent, and not resolvable. In the current experiments, only an ultrafast rise time is observable in the ground state and fitting the slower rise time component is obscured by our high noise. The prior experiments monitored both the $v = 1 \rightarrow v = 2$ and $v = 2 \rightarrow v = 3$ vibrational transitions while our higher concentrations made it more difficult to monitor these transitions due to line width overlap of the ground-state bleach. It is possible that in the prior experiments the $v = 1 \rightarrow v = 2$ transition did not properly account for the bleach component, thereby distorting the rise time to make it appear longer than for the $v = 2 \rightarrow v = 3$ transition. Another contributing effect would be the contribution of coherence artifacts in the rise time, which become much worse as the probe infrared wavelength approaches the ground-state frequency.

In summary, we believe that the new data and old data for ET rate as a function of vibrational quantum number are reasonably self-consistent when the experimental differences are understood by simulation.

V. Conclusions

We have reexamined our earlier report of electron transfer in the radical pair [Co(Cp)₂|V(CO)₆] using ultrafast infrared transient absorption spectroscopy. The radical pair is created from the ion pair by ultrafast visible charge-transfer excitation. We observe two major direct ET components with lifetimes of ~700 fs and ~5 ps. A small ~75 ps ET component is also observable and is due to some separation and re-formation of the radical pairs. Recovery of the ion-pair ground state shows that both fast components are due to ET rather than vibrational relaxation in the radical-pair state. Spectral modeling indicates that the two fast ET components are assignable to two ion-pair contact geometries with charge-transfer absorption origins different by about 1250 ± 350 cm^{-1}. The ~700 fs ET lifetime depends on the vibrational quantum state of the nontotally symmetric CO stretch in the V(CO)₆ radical, where the lifetime decreases by ~10% for the first vibrational quantum and ~45% for the second quantum. There is no quantum effect for the 5 ps ET component. Standard ET rate models cannot explain the rate dependence for a nontotally symmetric mode, and we assign it as a breakdown of the Condon approximation.

We find that the IVR time to transfer vibrational energy from the totally symmetric to the nontotally symmetric CO stretch is less than 75 fs for a 1-quantum IVR process. We observe a ~200 fs rise time for 2-quantum IVR for excitation wavelengths of 800 and 700 nm. An apparent change in the ET kinetics occurs when charge-transfer excitation wavelengths are decreased to 620 and 555 nm. At higher excitation energies all quantum levels show a 200 fs rise time, which is unexpected for the zero quantum level. We assign this effect to the onset of sufficient internal vibrational energy in low-frequency vibrations to cause geometric interconversion between energetically similar Jahn–Teller geometries in the V(CO)₆ radical. The rise time reflects the time for the V(CO)₆ radical species to assume a stable geometry by VR of low-frequency vibrations.

The hypothesis of two ion-pair geometries leading to different ET rates is supported by the transient absorbance data, where the relative amplitudes of the two rate components change with excitation frequency. Further examination of the charge-transfer absorption band via time-dependent Raman analysis and Franck–Condon calculations confirms that two absorptions could exist under the single broad band, but a theory of asymmetric inhomogeneous line broadening is required to make a more complete analysis. Other inadequacies of the model suggest that re-excitation of vibrationally hot ion pairs is probably contributing to populations of larger quantum numbers during the pump pulse.

These results demonstrate that earlier measurements from our group on the same molecule had insufficient time resolution to observe the fast ET component and thereby inferred a vibrational quantum effect in a single ET rate component rather than in the ultrafast ET component.

References and Notes

(1) Meyer, T. J. *Prog. Inorg. Chem.* **1983**, *30*, 389.

(2) Newton, M. D.; Sutin, N. *Annu. Rev. Phys. Chem.* **1984**, *35*, 437.

(3) Marcus, R. A.; Sutin, N. *Biochim. Biophys. Acta* **1985**, *811*, 265.

(4) *Electron Transfer in Inorganic, Organic, and Biological Systems*; Bolton, J. R., Mataga, N., McLendon, G., Eds.; American Chemical Society: Washington, DC, 1991; p 295.

(5) Newton, M. D.; Zhong, E. *J. Phys. Chem.* **1991**, *95*, 2317.

(6) Barbara, P. F.; Meyer, T. J.; Ratner, M. A. *J. Phys. Chem.* **1996**, *100*, 13148.

(7) Bixon, M.; Jortner, J. Electron Transfer − From Isolated Molecules to Biomolecules. In *Electron Transfer-From Isolated Molecules to Biomolecules, Pt 1*; John Wiley & Sons, Inc.: New York, 1999; Vol. 106, p 35.

(8) Spears, K. G.; Wen, X.; Zhang, R. *J. Phys. Chem.* **1996**, *100*, 10206.

(9) Hush, N. S. *Prog. Inorg. Chem.* **1967**, *8*, 357.

(10) Spears, K. G.; Shang, H. *J. Phys. Chem. A* **2000**, *104*, 2668.

(11) Edgell, W. F.; Hegde, S.; Barbetta, A. *J. Am. Chem. Soc.* **1978**, *100*, 1406.

(12) Bernier, J. C.; Kahn, O. *Chem. Phys. Lett.* **1973**, *19*, 414.

(13) Brunschwig, B. S.; Sutin, N. *Commun. Inorg. Chem.* **1987**, *6*, 209.

(14) Spears, K. G. *J. Phys. Chem.* **1995**, *99*, 2469.

(15) Marin, T. W.; Homoelle, B. J.; Spears, K. G.; Hupp, J. T.; Spreer, L. O. *J. Phys. Chem. A*, in press.

(16) Bockman, T. M.; Kochi, J. K. *J. Am. Chem. Soc.* **1989**, *111*, 4669.

(17) Keller, H. J.; Laubereau, P.; Nöthe, D. *Z. Naturforsch.* **1969**, *24*, 257.

(18) Wynne, K.; Hochstrasser, R. M. *Chem. Phys.* **1995**, *193*, 211.

(19) Lian, T.; Bromberg, S. E.; Asplund, M. C.; Yang, H.; Harris, C. B. *J. Phys. Chem.* **1996**, *100*, 11994.

(20) Spears, K. G.; Wen, X.; Arrivo, S. M. *J. Phys. Chem.* **1994**, *98*, 9693.

(21) Lucia, L. A.; Abboud, K.; Schanze, K. S. *Inorg. Chem.* **1997**, *36*, 6224.

(22) Dougherty, T. P.; Heilweil, E. J. *J. Chem. Phys.* **1994**, *100*, 4006.

(23) Kenkre, V. M.; Tokmakoff, A.; Fayer, M. D. *J. Chem. Phys.* **1994**, *101*, 10618.

(24) Tokmakoff, A.; Sauter, B.; Kwok, A. S.; Fayer, M. D. *Chem. Phys. Lett.* **1994**, *221*, 412.

(25) Moore, P.; Tokmakoff, A.; Keyes, T.; Fayer, M. D. *J. Chem. Phys.* **1995**, *103*, 3325.

(26) Arrivo, S. M.; Dougherty, T. P.; Grubbs, W. T.; Heilweil, E. J. *Chem. Phys. Lett.* **1995**, *235*, 247.

(27) Kambhampati, P.; Son, D. H.; Kee, T. W.; Barbara, P. F. *J. Phys. Chem. A* **2000**, *104*, 10637.

(28) Wang, C. F.; Mohney, B. K.; Akhremitchev, B. B.; Walker, G. C. *J. Phys. Chem. A* **2000**, *104*, 4314.

(29) Ito, T.; Hamaguchi, T.; Nagino, H.; Yamaguchi, T.; Washington, J.; Kubiak, C. P. *Science* **1997**, *277*, 660.

(30) Ito, T.; Hamaguchi, T.; Nagino, H.; Yamaguchi, T.; Kido, H.; Zavarine, I. S.; Richmond, T.; Washington, J.; Kubiak, C. P. *J. Am. Chem. Soc.* **1999**, *121*, 4625.

(31) Zavarine, I. S.; Kubiak, C. P.; Yamaguchi, T.; Ota, K.; Matsui, T.; Ito, T. *Inorg. Chem.* **2000**, *39*, 2696.

(32) Frisch, M. J.; Trucks, G. W.; Schlegel, H. B.; Scuseria, G. E.; Robb, M. A.; Cheeseman, J. R.; Zakrzewski, V. G.; Montgomery, J. A., Jr.; Stratmann, R. E.; Burant, J. C.; Dapprich, S.; Millam, J. M.; Daniels, A. D.; Kudin, K. N.; Strain, M. C.; Farkas, O.; Tomasi, J.; Barone, V.; Cossi, M.; Cammi, R.; Mennucci, B.; Pomelli, C.; Adamo, C.; Clifford, S.; Ochterski, J.; Petersson, G. A.; Ayala, P. Y.; Cui, Q.; Morokuma, K.; Malick, D. K.; Rabuck, A. D.; Raghavachari, K.; Foresman, J. B.; Cioslowski, J.; Ortiz, J. V.; Stefanov, B. B.; Liu, G.; Liashenko, A.; Piskorz, P.; Komaromi, I.; Gomperts, R.; Martin, R. L.; Fox, D. J.; Keith, T.; Al-Laham, M. A.; Peng, C. Y.; Nanayakkara, A.; Gonzalez, C.; Challacombe, M.; Gill, P. M. W.; Johnson, B. G.; Chen, W.; Wong, M. W.; Andres, J. L.; Head-Gordon, M.; Replogle, E. S.; Pople, J. A. *Gaussian 98*, revision A.7; Gaussian, Inc.: Pittsburgh, PA, 1998.

(33) Heller, E. J. *Acc. Chem. Res.* **1981**, *14*, 368.

(34) Heller, E. J.; Sundberg, R. L.; Tannor, D. *J. Phys. Chem.* **1982**, *86*, 1822.

(35) Tannor, D. J.; Heller, E. J. *J. Chem. Phys.* **1982**, *77*, 202.

(36) Myers, A. B.; Mathies, R. A. Resonance Raman Intensities: A Probe of Excited-State Structure and Dynamics. In *Biological Applications of Raman Spectroscopy*; Spiro, T. B., Ed.; John Wiley and Sons: New York, 1987; Vol. 2, p 1.

(37) Shin, K.-S. K.; Zink, J. I. *Inorg. Chem.* **1989**, *28*, 4358.

(38) Zink, J. I.; Shin, K.-S. K. Molecular Distortions in Excited Electronic States Determined from Electronic and Resonance Raman Spectroscopy. In *Advances in Photochemistry*; Volman, D. H., Hammond, G. S., Neckers, D. C., Eds.; John Wiley and Sons: New York, 1991; Vol. 16, p 119.

(39) Myers, A. B. Excited Electronic State Properties from Ground-State Resonance Raman Intensities. In *Laser Techniques in Chemistry*; Myers, A. B., Rizzo, T. R., Eds.; John Wiley and Sons: New York, 1995; Vol. XXIII, p 325.

(40) Myers, A. B. *Chem. Rev.* **1996**, *96*, 911.

(41) Myers Kelly, A. B. *J. Phys. Chem. A* **1999**, *103*, 6891.

(42) Mukamel, S.; Yan, Y. J. In *Recent Trends in Raman Spectroscopy*; Banerjee, S. B. J., Ed.; World Scientific: Singapore, 1989; p 160.

(43) Bosma, W. B.; Yan, Y. J.; Mukamel, S. *Phys. Rev. A* **1990**, *42*, 6920.

(44) Mukamel, S. *Annu. Rev. Phys. Chem.* **1990**, *41*, 647.

(45) Sando, G. M.; Spears, K. G.; Hupp, J. T.; Ruhoff, P. T. *J. Phys. Chem. A* **2001**, *105*, 5317.

(46) Heitele, H. *Angew. Chem., Int. Ed. Engl.* **1993**, *32*, 359.

(47) McManis, G. E.; Golovin, M. N.; Weaver, M. J. *J. Phys. Chem.* **1986**, *90*, 6563.

(48) Nielson, R. M.; McManis, G. E.; Golovin, M. N.; Weaver, M. J. *J. Phys. Chem.* **1988**, *92*, 3441.

(49) Sando, G. M.; Spears, K. G. *J. Phys. Chem. A* **2001**, *105*, 5326.